Journal of Catalysis 270 (2010) 136–145

Contents lists available at ScienceDirect

Journal of Catalysis

journal homepage: www.elsevier.com/locate/jcat

Nanostructured Pt- and Ni-based catalysts for CO_2-reforming of methane

M. García-Diéguez, I.S. Pieta, M.C. Herrera, M.A. Larrubia, L.J. Alemany *

Departamento de Ingeniería Química, Facultad de Ciencias, Campus de Teatinos, Universidad de Málaga, Málaga E-29071, Spain

ARTICLE INFO

Article history:
Received 18 August 2009
Revised 7 December 2009
Accepted 13 December 2009
Available online 29 January 2010

Keywords:
Dry reforming
Methane
Nickel
Platinum

ABSTRACT

The effect of using a nanofibrous Al_2O_3 as support for Ni-based catalysts, modified with Pt, for the dry reforming of methane (DRM) was studied. Monometallic (Ni and Pt) and bimetallic (PtNi) supported catalysts were synthesized, characterized (XRD, TEM, XPS, Raman and Elemental Analysis) and tested under DRM conditions. A monometallic Pt catalyst supported on a commercial alumina was also prepared and studied for comparative purposes. Characterization results showed that the nanofibrous alumina allowed nanostructured systems with Pt and Ni particles well dispersed, avoiding metal sintering. Additionally, Pt addition promoted the formation of NiO, instead of $NiAl_2O_4$, and facilitated its reduction to Ni^0 during the catalysts activation. It was also observed that the average size of Ni^0 particles decreased with increasing Pt content. Activity tests demonstrated that Pt presence and the use of the nanofibrous support in Ni catalysts improve CH_4 and CO_2 conversions, reaching values close to equilibrium. Moreover, Pt inhibits coke deposition and reduces the operation temperature. From stability tests it can be concluded that Pt enhances the stability of Ni-based catalysts for DRM.

1. Introduction

Recently, there has been a lot of interest in light hydrocarbons' CO_2-reforming, due to the use of synthesis gas as feedstock for several chemical processes, i.e. fuel cells, methanol synthesis and Fischer–Tropsch reaction [1–7]. Furthermore, dry reforming could be an alternative route to convert Natural Gas into products of higher value. The CO_2-reforming of methane (DRM) is a process being developed for the production of syngas and CO. It has been combined with steam to reform Natural Gas streams containing CO_2 or used in processes where a CO_2 recycle is desirable. Additionally, DRM provides low H_2/CO ratios required for hydroformylation and carbonylation reactions.

The commonly used catalysts for dry reforming are Ni-based catalysts. Unfortunately, under reforming conditions, Ni catalysts tend to form Ni clusters and unreactive carbon that could block the catalysts pores and encapsulate the active sites, which would lead to quick catalyst deactivation [3,8–10]. However, carbon formation can be reduced or suppressed by controlling the reaction kinetically using adequate metals and supports. It is well known that noble metals inhibit coke formation, and the carbon obtained differs in nature from that formed over Ni catalysts. Moreover, it has been reported that a small amount of noble metals can promote the reducibility of the base metal, such as Ni, and stabilize its degree of reduction during the catalytic process [11–13].

Chen et al. [11] studied the promoting effect of Pt, Pd and Rh in $Ni_{0.03}Mg_{0.97}O$ catalysts for CO_2-reforming. They found that the noble metal addition improves the catalyst stability and reducibility. Tomishige et al. [14] observed that the catalytic activity increased, in autothermal reforming of methane, when small amounts of Pt were incorporated to Ni/Al_2O_3 catalysts. Pawelec et al. [3] reported that, in bimetallic PtNi catalysts supported on ZSM-5 for DRM, the presence of Pt (0.5%) leads to the formation of small and reducible nano-sized NiO particles. They also observed an improvement in the catalytic activity and stability, which was attributed to an increase in the nickel metallic dispersion caused by intimate contact between nickel and platinum.

Surface structure and surface acidity affect carbon deposition in DRM. Thus, by controlling the size of the metal ensembles and the acidity of the support it is possible to control the carbon formation [15]. It has been reported that when a metal is supported on a metal oxide with a strong Lewis basicity, the net carbon formation decreases. Besides, the superficial characteristics and the morphology of the support influence the metal–support interaction, affecting the metal dispersion and reducibility, as well as the catalytic activity and stability [16]. An appropriate support should be able to improve the dispersion of active components, promote effective metal–support interactions and retain the unique properties of the impregnated metals [17]. It has been studied by Martínez et al. [18] the use of a nanofibrous alumina as support for RuCo catalysts for Fischer–Tropsch process, which allows lower Co particle size and higher dispersion values than others commercial aluminas.

The aim of the present work is to develop stable Ni-containing catalysts with resistance to coke deposition and good performance under reforming conditions. The effect of using an alumina with nanofibrous morphology as support for Ni-based catalysts, as well

* Corresponding author. Fax: +34 952 13 1919.
E-mail address: luijo@uma.es (L.J. Alemany).

0021-9517/$ - see front matter © 2009 Elsevier Inc. All rights reserved.
doi:10.1016/j.jcat.2009.12.010

as the addition of different loads of Pt, was studied. The materials were characterized by conventional methods. The catalytic activity and stability were evaluated, for all the catalysts, under dry reforming conditions at steady state.

2. Experimental

2.1. Catalysts preparation

A synthesized nanostructured γ-Al_2O_3 (denoted as Al_2O_3(N)) and a commercial γ-Al_2O_3 Puralox SCCa-5/200 from Sasol (denoted as Al_2O_3(S)) were employed as supports. The nanostructured alumina was prepared using $NaAlO_2$ as precursor. An aqueous $NaAlO_2$ solution was added dropwise to 5 N acetic acid solution. The precipitate obtained was decanted, filtered and washed with water. The white powder was dried overnight at 100 °C and subsequently mixed with a non-ionic surfactant (Tergitol 15-TS-5, Sigma) using a Tergitol/Al ratio of 0.5. The mixture was maintained in an autoclave for 72 h at 100 °C and later calcined at 500 °C for 20 h [16,19]. Before supports' characterization and catalysts' preparation, both of the supports were calcined in air at 800 °C for 2 h (10 °C/min).

Bimetallic catalysts supported on the nanofibrous alumina (Pt [0.04–0.4 at/nm^2]–Ni [4 at/nm^2]; denoted as *x*Pt4Ni/Al_2O_3(N)) where *x* is the Pt load expressed in terms of atomic superficial density, to compare in terms of surface coverage) were prepared by simultaneous incipient wetness impregnation of the support, with a solution of diaminedinitroplatinum and/or nickel nitrate. The impregnation was done in a single step. The support impregnated was dried at 100 °C for 2 h and calcined at 600 °C for 2 h (10 °C/min). Monometallic Pt and Ni catalysts supported on the Al_2O_3(N) (Pt [0.4 at/nm^2] and Ni [4 at/nm^2]; denoted as 0.4Pt/Al_2O_3(N) and 4Ni/Al_2O_3(N)), and a monometallic Pt catalyst supported on the commercial alumina (Pt [0.4 at/nm^2]; denoted as 0.4Pt/Al_2O_3(S)) were also prepared. The synthesized catalysts and their identification are summarized in Table 1.

2.2. Characterization

X-ray Powder Diffraction data have been recorded with an X'Pert MPD PRO diffractometer (PANalytical) using Cu Kα1 radiation (λ = 1.54059 Å) and a Ge(1 1 1) primary monochromator. The X-ray tube worked at 45 kV and 35 mA. The measurements were done from 10° to 70° (2θ). X-ray Photoelectron Spectra were recorded on a Physical Electronic 5701 spectrometer equipped with a PHI 10-360 analyzer using the Mg K_α X-ray source. Binding Energy (BE) values were referred to the C1s peak (284.8 eV) from the adventitious carbon for the catalysts before reaction and to the Al 2p peak for the catalysts after reaction. All deconvolutions of experimental curves were done with Gaussian and Lorenzian line fitting, minimizing the (χ^2) chi-square values. N_2 adsorption–desorption isotherms for the supports were registered at −196 °C using a Beckman Coulter SA3100 Surface Area Analyzer. Before the analysis, the samples were outgassed in vacuum (1.10^{-3} Pa) for 5 h at 180 °C. The specific surface area was obtained by the BET equation and the pore volume by the BJH method. TEM images were taken with a Philips CM 200 of 200 kV; the samples were prepared using ethanol as dispersant. The carbon content of the catalysts after reaction was obtained *via* elemental analysis technique using an Elemental Analyzer, Perkin–Elmer 2400 CHN. Raman spectra were recorded on a Bruker-Senterra Raman imagine microscope with the 532 nm Nd–YAg laser and a CCD detector. Each spectrum was collected at room temperature under 10 mW of laser power.

Table 1
Theoretical metal content and atomic metal density of the catalysts.

Catalyst	Metal density (at/nm^2)		Metal content (wt.%)		Pt/Ni[a]
	Ni	Pt	Ni	Pt	
4Ni/Al_2O_3(N)	4	0	10	0	0
0.04Pt4Ni/Al_2O_3(N)	4	0.04	10	0.4	1/100
0.4Pt4Ni/Al_2O_3(N)	4	0.4	10	4	1/10
0.4Pt/Al_2O_3(N)	0	0.4	0	4	∞
0.4Pt/Al_2O_3(S)	0	0.4	0	2	∞

[a] Theoretical atomic ratio.

2.3. Reactivity

Steady-state experiments were carried out in a Microactivity-Reference reaction system from PID Eng&Tech (Spain) at atmospheric pressure in a temperature range between 400 and 700 °C. A tubular fixed-bed stainless steel reactor (i.d. 9 mm) with 100 mg of catalyst (250–420 μm) was employed. The total gas flow rate was kept constant at 50 N cm^3/min with stoichiometric composition diluted in He (CH_4/CO_2/He = 20/20/60). The space velocity and the contact time were 6000 h^{-1} and 0.8 g h mol^{-1}, respectively; operating under plug flow conditions. Preliminary reactivity tests with different catalyst particle sizes and dilutions, measuring the radial and axial temperatures at different points, were performed to confirm the non-existence of heat or mass transfer limitations. Before reaction, catalysts were activated in situ with H_2 (3% in He, 30 N cm^3 min^{-1}) at 700 °C for 2 h. The reaction temperature was measured with a thermocouple placed in the reactor bed. The reactor effluent was analyzed by GC (Agilent 4890D) equipped with TCD and FID detectors. Stability runs were performed at 700 °C at the same reaction conditions as in the activity tests. C, H and O balances were closed with deviations lower than 5%.

3. Results and discussion

3.1. Characterization

The XRD profile and the TEM images of both of the supports, calcined at 800 °C, are shown in Fig. 1. It can be noticed that both supports present the characteristic features of a γ-alumina (JCPDS 75-0921). Additionally, it is interesting to observe, in the TEM micrographs, the morphological differences between both of the aluminas; where the Al_2O_3(N) exhibits a nanofibrous morphology, with fibers of less than 2 nm in diameter. Results from N_2 adsorption–desorption revealed that the Al_2O_3(N) presented high surface area (A_{BET} = 300 m^2 g^{-1}) and pore volume (V_P = 1 cm^3 g^{-1}); while, the commercial Al_2O_3(S) presented lower surface area and pore volume values (A_{BET} = 160 m^2 g^{-1} and V_P = 0.7 cm^3 g^{-1}). The textural properties as well as the nanofibrous structure of the Al_2O_3(N) were stable up to 1000 °C, which is desirable for the DRM. Normally, at high temperature the γ-alumina tends to lose its surface area, causing the sintering of the surface active species. A good support should possess high surface area and mechanical strength in addition to being thermally stable [17]. In reference to the surface area and pore volume values of the catalysts after reaction, it has been registered for the catalyst with the highest metal load that the surface area (189 m^2 g^{-1}) and the pore volume (0.8 cm^3 g^{-1}) decrease in ∼30% and in ∼20%, respectively. The reduction in the surface area value is associated with the surface coverage (4.4 at/nm^2) of the alumina.

In Fig. 2 are presented the XRD patterns of the catalysts before reaction. The diffractions peaks associated with γ-Al_2O_3 in the Ni-containing catalysts have a shift to a lower Bragg angle, suggesting

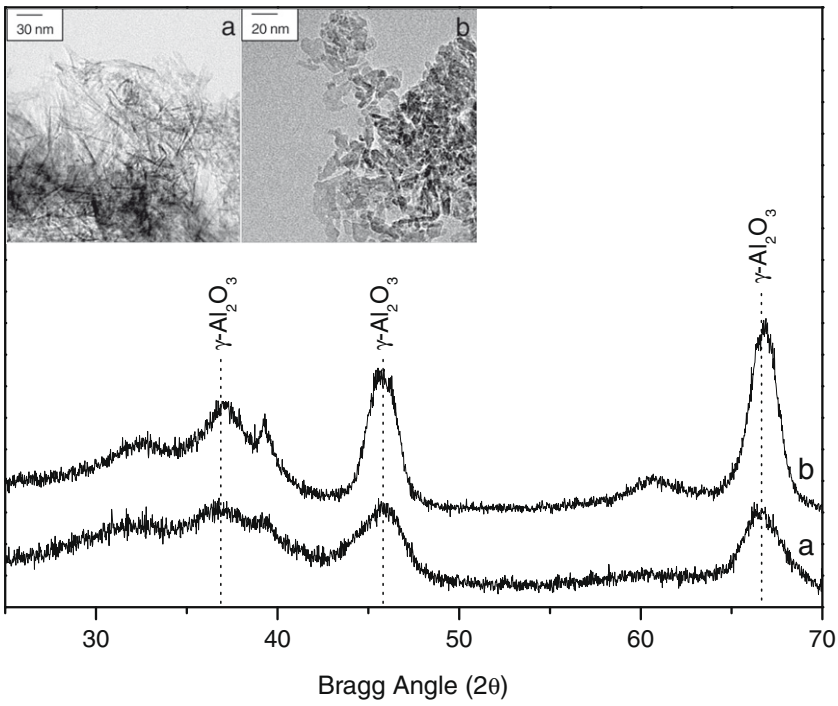

Fig. 1. XRD profiles and TEM images of both aluminas. (a) 0.4Pt/Al_2O_3(N) and (b) 0.4Pt/Al_2O_3(S).

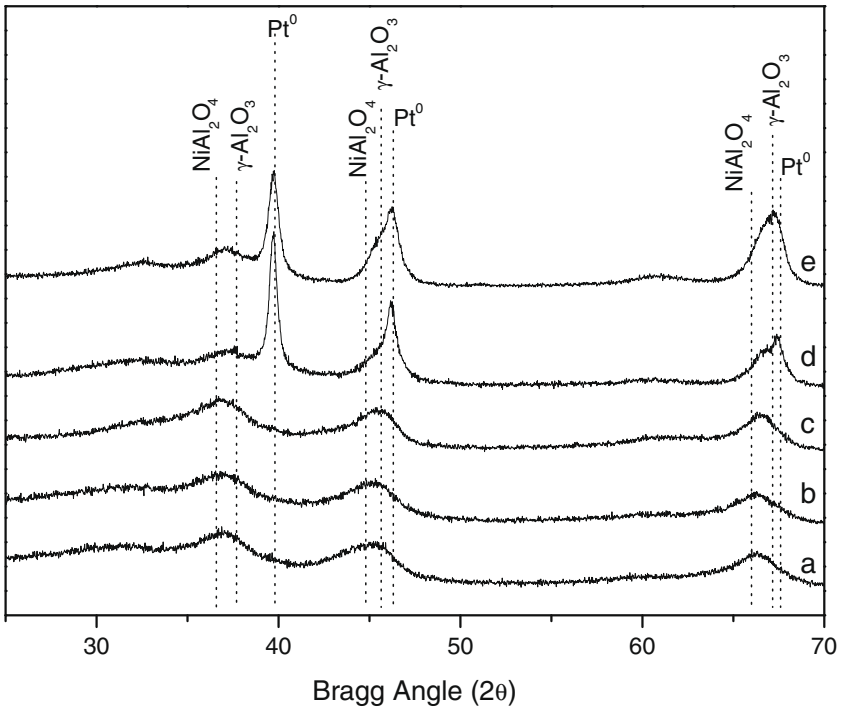

Fig. 2. XRD diffractograms of calcined catalysts. (a) 4Ni/Al_2O_3(N); (b) 0.04Pt4Ni/Al_2O_3(N); (c) 0.4Pt4Ni/Al_2O_3(N); (d) 0.4Pt/Al_2O_3(N) and (e) 0.4Pt/Al_2O_3(S).

the presence of $NiAl_2O_4$ (JCPDS 01-1299). Peaks related to metallic Ni or NiO were not detected, which could indicate that if these species were present, they would be quite small or in a low quantity to be detected by XRD. Similarly, signals associated with Pt were not registered in the XRD patterns of the bimetallic catalysts either. Moreover, for the Ni-free catalyst (0.4Pt/Al_2O_3(N) and 0.4Pt/Al_2O_3(S)), signals superimposed on the γ-Al_2O_3 were detected, associated with Pt^0 (JCPDS 01-1190). Pt^0 was formed during the calcination procedure of the catalysts at high temperature. The average size of Pt^0 particles, calculated by the Scherrer equation, was 11 nm and 13 nm for the 0.4Pt/Al_2O_3(N) and 0.4Pt/Al_2O_3(S) catalysts, respectively.

The XRD patterns of the catalysts after reaction are shown in Fig. 3. First, it is interesting to observe that the XRD profile of the 0.4Pt/Al_2O_3(N) and the 0.4Pt/Al_2O_3(S) catalysts did not show any modification with respect to the ones registered before reaction,

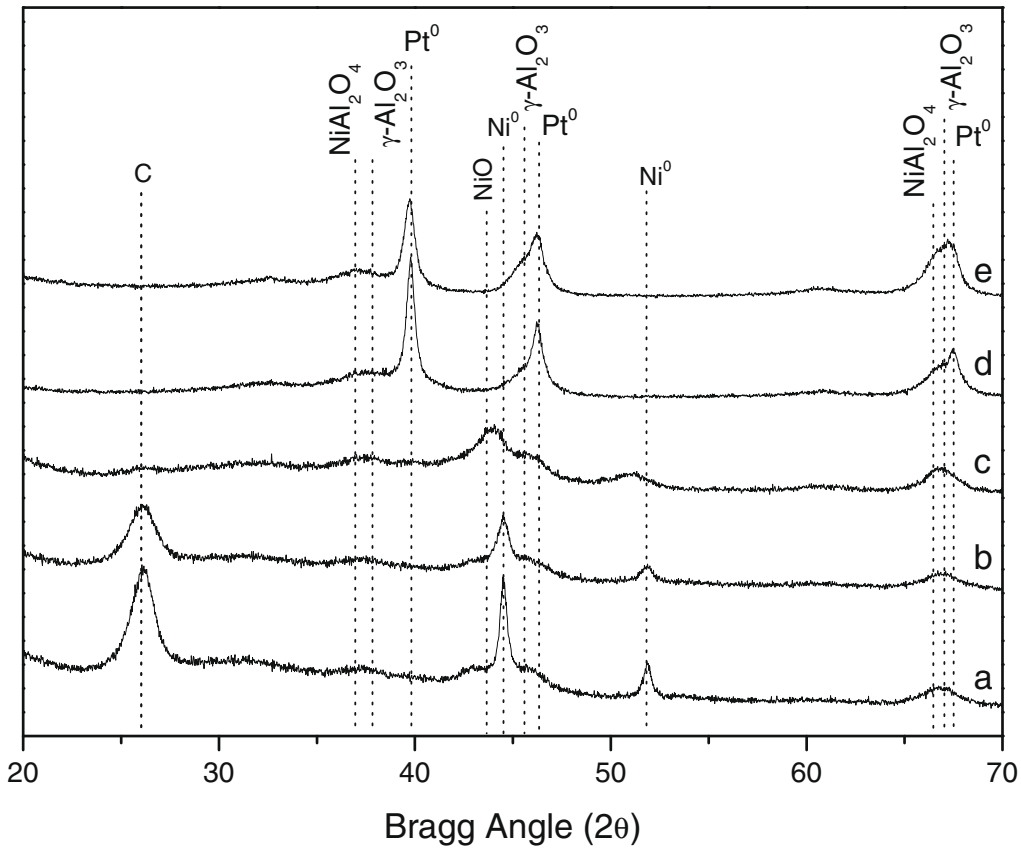

Fig. 3. XRD diffractograms of catalysts after reaction. (a) 4Ni/Al_2O_3(N); (b) 0.04Pt4Ni/Al_2O_3(N); (c) 0.4Pt4Ni/Al_2O_3(N); (d) 0.4Pt/Al_2O_3(N) and (e) 0.4Pt/Al_2O_3(S).

where signals related to Pt^0 and the support (γ-Al_2O_3) were only detected; changes in the average particle size of Pt^0 were not observed either. However, it is worth noticing that after reaction all of the Ni-containing catalysts presented signals related to Ni^0 (JCPDS 70-1849). The peak width of these signals was modified with the Pt/Ni ratio, indicating that the Ni particle size changed as a function of the Pt load. The average Ni^0 particle sizes, calculated by the Scherrer equation and estimated by TEM, as well as the Ni dispersion values, assuming spherical and uniform particles for the Ni-containing catalysts after reaction, are presented in Table 2. It can be observed that when the Pt amount increased, the Ni^0 particle size decreased considerably and the Ni dispersion increased in agreement with data reported in the literature for RhNi catalysts supported on alumina used in DRM [20] and for PtNi catalysts supported on silica for the hydrogenation of benzene [21]. The addition of Pt and the morphology of the support affected the Ni redispersion, decreasing the mobility of the Ni metal particles. Moreover, in the Ni-containing catalysts after reaction XRD signals associated with graphitic carbon (JCPDS 89-8491) and NiO (JCPDS 65-6920) were also observed.

Table 2
Average particle size and dispersion of Ni^0 in the catalysts after reaction.

Catalyst	D_PNi^0 (nm)[a]	D (%)[b]	D_PNi^0 (nm)[c]
4Ni/Al_2O_3(N)	23	4.2	25
0.04Pt4Ni/Al_2O_3(N)	13	7.5	14
0.4Pt4Ni/Al_2O_3(N)	7	13.9	10

[a] Calculated by the Scherrer equation.
[b] Metal dispersion (XRD).
[c] Estimated by TEM.

Carbon deposition on catalysts for the DRM can lead to high rates of catalyst deactivation; the net carbon formation in the PtNi catalysts supported on the nanofibrous alumina was studied. The carbon contents (expressed as wt.%) as a function of the theoretical Pt/Ni atomic ratio in the catalysts after reaction obtained by CHN analysis are presented in Fig. 4A. It can be inferred that, as well as the D_PNi^0, the carbon content, measured over the catalysts after reaction, depends on the Pt load. The same trend was observed by XPS (Fig. 4B), where the atomic carbon content over the catalysts' surface seems to be dependent on the amount of Pt. Moreover, the increment of the carbon concentration in the catalysts after reaction also decreased when the Pt/Ni ratio increased, varying from 1% to 68% in the 4Ni/Al_2O_3(N) catalyst (Pt/Ni = 0), while for the Ni-free catalyst (Pt/Ni = ∞) no variation in the carbon content was observed. For the 0.4Pt/Al_2O_3(S) catalyst, the carbon content after reaction (CHN-analysis) was minimal, and no variation in the carbon content was detected. It has been already reported by Rostrup-Nielsen [22] that the ensembles necessary for carbon formation are larger than those for DRM.

TEM images supporting the previous observations for the catalysts before and after reaction are presented in Figs. 5 and 6, respectively. It can be noticed that, for the Ni-based catalysts before reaction, only the nanofibrous morphology of the alumina was observed; Ni or Pt metallic particles could not be detected. For the monometallic 0.4Pt/Al_2O_3(N) and 0.4Pt/Al_2O_3(S) catalysts, apart from the support, metallic Pt particles close to 12 nm and 10–30 nm could also be registered.

Furthermore, it is worth noticing that, for the catalysts after reaction, there is a considerable difference in carbon formation. Apparently, the 0.4Pt/Al_2O_3(N) and the 0.4Pt/Al_2O_3(S) catalysts with the lowest carbon content, registered by elemental analysis, did not form carbon structures. In addition, for the 0.4Pt/Al_2O_3(S)

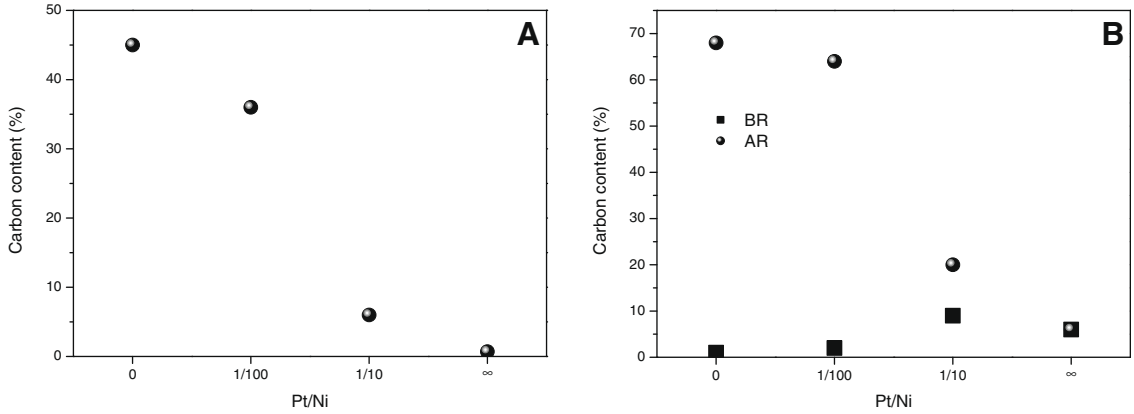

Fig. 4. Carbon content in the catalysts. (A) After reaction (Elemental Analysis – wt.%); (B) before (BR) and after reaction (AR) (XPS – superficial atomic concentration %).

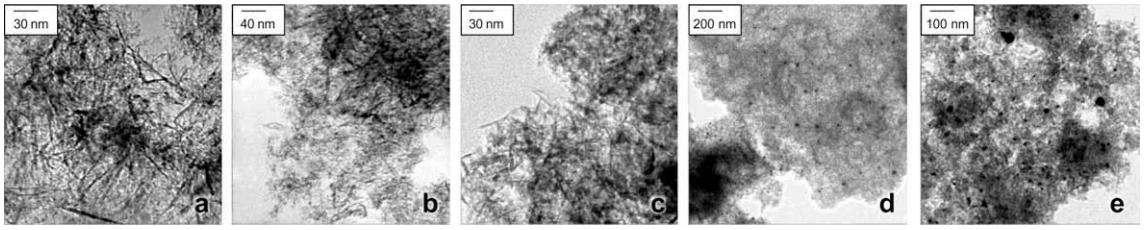

Fig. 5. TEM images of catalysts before reaction. (a) 4Ni/Al_2O_3(N); (b) 0.04Pt4Ni/Al_2O_3(N); (c) 0.4Pt4Ni/Al_2O_3(N); (d) 0.4Pt/Al_2O_3(N) and (e) 0.4Pt/Al_2O_3(S).

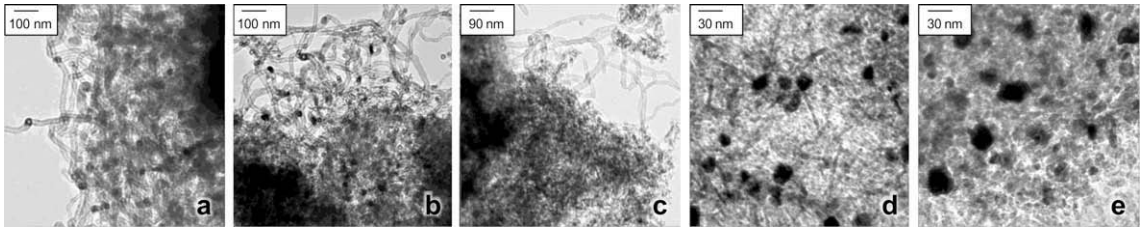

Fig. 6. TEM images of catalysts after reaction. (a) 4Ni/Al_2O_3(N); (b) 0.04Pt4Ni/Al_2O_3(N); (c) 0.4Pt4Ni/Al_2O_3(N); (d) 0.4Pt/Al_2O_3(N) and (e) 0.4Pt/Al_2O_3(S).

some Pt aggregates could be observed, contrary to what occurs with the 0.4Pt/Al_2O_3(N), where apparently the Pt particles are homogenously distributed over the support. This result suggests that the morphology and the superficial characteristics of the nanofibrous alumina favor the stabilization of the metal particles after reaction.

The TEM images of the 4Ni/Al_2O_3(N) and the 0.04Pt4Ni/Al_2O_3(N) catalysts showed the formation of carbon nanotubes (CNTs) and carbon nanofibers (CNFs), being the relative contribution of coke greater for the 4Ni/Al_2O_3(N) catalyst than for the 0.04Pt4Ni/Al_2O_3(N). This observation is in agreement with the Raman spectra obtained for the catalysts after reaction (Fig. 7).

The Raman spectrum of the 0.4Pt/Al_2O_3(N) catalyst (Pt/Ni = ∞) did not present any signal related to carbon. However, the Raman spectrum of the 0.4Pt4Ni/Al_2O_3 catalyst (Pt/Ni = 1/10), in the 1200–1700 cm^{-1} region, presented two weak and symmetrical signals centered at 1337 cm^{-1} and 1588 cm^{-1} related to the defect mode (signal D) and to the graphite mode (signal G) [23–25], which correspond to the modes associated with CNFs.

On the other hand, the Raman spectra registered for the 0.04Pt4Ni/Al_2O_3(N) (Pt/Ni = 1/100) and 4Ni/Al_2O_3(N) (Pt/Ni = 0) catalysts presented, two intense and non-symmetrical signals, suggesting the superposition of different types of carbon contributions. Deconvolutions of the Raman spectra were done, indicating the presence of signals at 1588–1337 cm^{-1} and at 1570–1348 cm^{-1} associated with CNFs and CNTs, respectively [23].

The C1s core level spectra of the catalysts after reaction are shown in Fig. 8. It can be observed that, for all of the catalysts, a signal at 284.8 eV associated with adventitious carbon was registered. For the 0.4Pt/Al_2O_3(N) and the 0.4Pt/Al_2O_3(S) catalysts only one additional signal at 282.3 eV related to carbon was detected, indicating that coke accumulation over the Pt-catalysts' surface was minimal as was observed by CHN analysis and Raman. Moreover, for the 0.4Pt4Ni/Al_2O_3(N) catalyst two additional contributions at 282.1 eV and at 280.2 eV were registered, which can be related to filamentous carbon and CNFs formed above the catalyst surface without physical contact, creating a differential charge effect, as was also reported by Pawelec et al. [3].

Furthermore, for the catalysts with low Pt content (0.04Pt4Ni/Al_2O_3(N) and 4Ni/Al_2O_3(N)), three additional signals related to carbon can be distinguished. The first one at 278.6 eV that could be assigned to CNTs formed over the catalysts' surface, which represents the highest relative contribution in both catalysts. The second signal at 279.6 eV related to CNFs [3] and the third signal, the weakest one, at 281.8 eV, associated with filamentous carbon. Signals related to C═O (~286.0 eV) and C—O (~288.4 eV) bonds were also

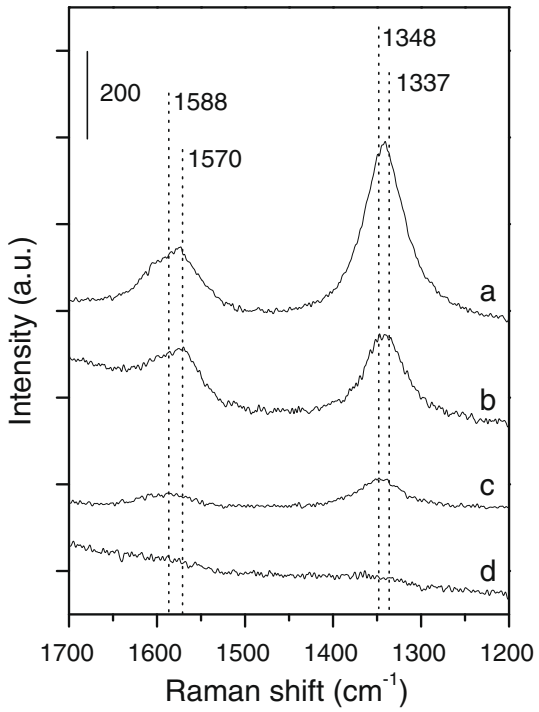

Fig. 7. Raman spectra of catalysts after reaction. (a) 4Ni/Al_2O_3(N); (b) 0.04Pt4Ni/Al_2O_3(N); (c) 0.4Pt4Ni/Al_2O_3(N) and (d) 0.4Pt/Al_2O_3(N).

detected for all of the catalysts after reaction, which were probably a product of the interaction between the CO_2 and the catalysts' surface; the relative contribution of this species was minimal. TEM, Raman and XPS results indicated that adding adequate Pt amounts, less than one or two orders of magnitude of the Ni atomic content, into Ni-based catalysts can inhibit the selectivity toward carbon deposition.

The Binding Energies and the surface atomic ratios of the Ni $2p_{3/2}$ and Pt $4d_{5/2}$ core electrons for the catalysts before and after reaction are summarized in Table 3. It can be seen that for all the Ni-based catalysts before reaction, two Ni species were detected: one registered at 855.2–855.3 eV related to Ni^{2+} as NiO and another one at 856.1–856.9 eV, which can be associated with the presence of Ni^{2+} as $NiAl_2O_4$ [26]. However, for the used Ni catalysts, three different signals were registered: at 852.9–853.1 eV related to Ni^0 [3,26], at 854.6–855.0 eV associated with Ni^{2+} as NiO and the last one at 856.1–856.6 eV that can be assigned to Ni^{2+} in the spinel form ($NiAl_2O_4$). The presence of NiO in the Ni catalysts after reaction indicates the oxidation of Ni during reaction, as was reported by Schuurman et al. [27] who considered the oxidation of Ni by CO_2 as an intermediate for the DRM over a Ni/SiO_2 catalyst. Catalyst characterization was not carried out in situ; thus, the oxidation of Ni during the catalyst transfer to the analysis system can also be considered. However, all the catalysts were manipulated in the same way, trying to avoid the contact of the samples with the air; the reoxidation during the samples' handling should have been minimal.

Furthermore, for the Pt-containing catalysts before reaction, two different signals associated with Pt^0 [3,28] (314.2–314.9 eV) and Pt^{2+} as PtO [29] (317.4–317.8 eV) were registered. The Pt^0/PtO ratio decreased with the Pt content and in the bimetallic PtNi catalysts. It has been reported by Navarro et al. [30] that the interaction between Pt and support or other metals produce changes in the relative superficial concentration of Pt^0. For the Pt-containing catalysts supported on the nanofibrous alumina after reaction, only one signal centered at 314.2–314.6 eV associated with Pt as Pt^0 was registered [3,27]. Moreover, for the 0.4Pt/Al_2O_3(S) after reaction two signals centered at 314.4 eV and 317.8 eV were detected, which are associated with Pt^0 and PtO, respectively.

Additionally, it is interesting to observe that Ni/Al surface atomic ratios (Table 3) decrease after reaction, which is less evident when the Pt content increases. This is opposite to what occurs with the Pt/Al surface atomic ratios, which do not change after reaction; with the exception of the 0.4Pt/Al_2O_3(S) catalyst, where the Pt/Al atomic ratio decreases 80% after reaction. These results suggest that metallic species are stabilized over the catalysts' surface by the nanofibrous alumina and Pt presence.

It is worth noticing that the Pt^0/PtO superficial atomic ratios in the monometallic Pt catalysts, before and after reaction, are higher when the nanofibrous support is employed, indicating that the use of the Al_2O_3(N) promotes the metal reducibility. The differences in the Pt particle size and in the Pt/Al and Pt^0/PtO atomic ratios for both of the Pt catalysts suggest that the metal–support interactions considerably vary. Furthermore, the $Ni^0/NiAl_2O_4$ and the Ni^0/NiO superficial atomic ratios for the Ni-containing catalysts increase with the Pt content. This latter observation indicates that the addition of Pt promotes the reducibility of Ni, which could be explained by a spillover effect of hydrogen from Pt to Ni, in agreement with the results reported by Chen et al. [11], using a NiO–MgO solid solution ($Ni_{0.03}Mg_{0.97}O$).

Results from XRD, XPS, Raman and elemental analysis indicate that the net carbon formation and the characteristics of the carbon formed can be related to the Ni particle size and dispersion but also

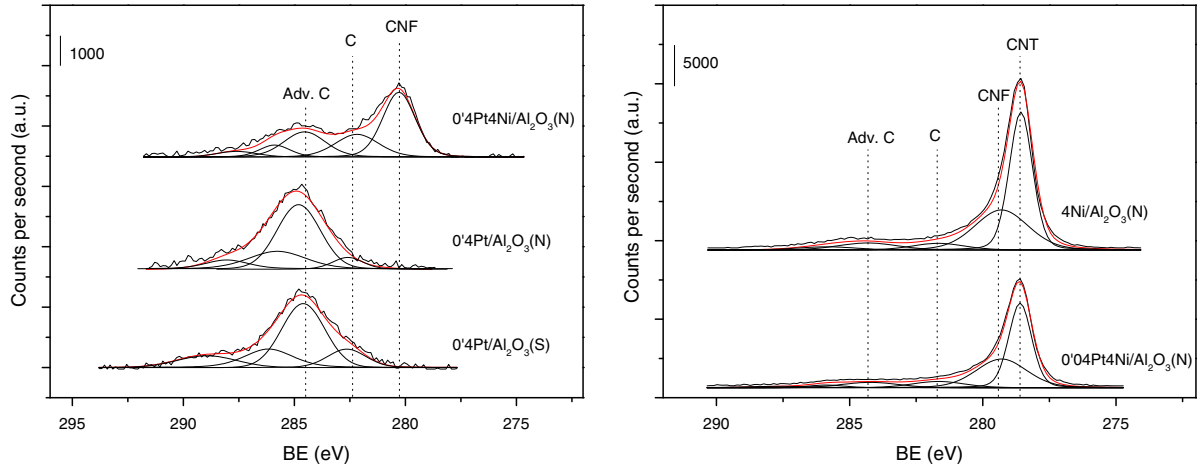

Fig. 8. C1s core level spectra of catalysts after reaction.

Table 3
BE and surface atomic ratios of catalysts, before (BR) and after (AR) reaction.

Catalyst	Ni $2p_{3/2}$[a]			Pt $4d_{5/2}$[a]		
		BR	AR		BR	AR
$4Ni/Al_2O_3(N)$	Ni^0	–	852.9 (25)	–	–	–
	NiO	855.3 (32)	854.6 (25)	–	–	–
	$NiAl_2O_4$	856.1 (68)	856.1 (50)	–	–	–
	Ni/Al[b]	0.09	0.02	–	–	–
$0.04Pt4Ni/Al_2O_3(N)$	Ni^0	–	853.1 (32)	Pt^0	314.2 (21)	314.6 (100)
	NiO	855.2 (34)	854.7 (20)	PtO	317.8 (79)	
	$NiAl_2O_4$	856.4 (66)	856.2 (48)			
	Ni/Al[b]	0.09	0.03	Pt/Al[b]	0.002	0.002
$0.4Pt4Ni/Al_2O_3(N)$	Ni^0	–	853.1 (35)	Pt^0	314.9 (42)	314.6 (100)
	NiO	855.2 (39)	855.0 (20)	PtO	317.5 (58)	–
	$NiAl_2O_4$	856.5 (61)	856.6 (45)			
	Ni/Al[b]	0.1	0.06	Pt/Al[b]	0.01	0.01
$0.4Pt/Al_2O_3(N)$	–	–	–	Pt^0	314.9 (87)	314.2 (100)
	–	–	–	PtO	317.4 (13)	–
	–	–	–	Pt/Al[b]	0.01	0.01
$0.4Pt/Al_2O_3(S)$	–	–	–	Pt^0	314.4 (75)	314.2 (100)
	–	–	–	PtO	317.8 (13)	
	–	–	–	Pt/Al[b]	0.01	0.002

[a] Binding Energies (±0.2 eV), in brackets () relative population of the species expressed in %.
[b] Surface atomic ratio.

to the Ni^0/NiO and $Ni^0/NiAl_2O_4$ ratios, parameters that are conditioned by the use of the nanofibrous support as well as the addition of Pt. It has been already reported that the carbon deposition is a process that depends on the metallic structure of the catalyst [31,15], being inhibited when small metallic particles are used [22]. The addition of Pt modifies the Ni ensembles, by a synergic effect, varying the dissociative adsorption capacity of methane and consequently reducing the net carbon formation. This fact together with the ability of Pt to remove carbon by CO_2 [32] could produce differences between the rates of carbon deposition and gasification by CO_2; at higher Pt content, higher carbon gasification and less net carbon formation.

On the other hand, some authors [20] have reported that the OH^- groups have an effect of decreasing the rate of coke deposition on metal, in our case the surface of alumina uncovered is almost the same for all of the PtNi catalysts; if the alumina had an direct effect on the global carbon formation, it would be similar for all of the catalysts. However, the alumina influences the nature of the metal–support interactions and the disposition of the active phase, factors that are related to the carbon deposition.

It is important to point out that there was no clear evidence, by XPS, TEM or XRD, of Ni–Pt alloy formation; however, it is clear that a kind of Pt–Ni interaction exists, which is responsible for changing the rate of the net carbon formation and for promoting the reducibility and stability of the Ni species.

3.2. Reactivity

The conversion values of CH_4 and CO_2, registered in the temperature range studied, are presented in Fig. 9, as well as the equilibrium conversions calculated, considering simultaneous CO_2–CH_4 reforming and reverse water gas shift reaction (RWGS) at the reactivity test conditions (atmospheric pressure and $CH_4/CO_2/He = 20/20/60$). Equilibrium calculations were done by the minimization of Gibbs Energy taking into account CH_4, CO_2, H_2, CO, H_2O and He as species in the system, solid carbon was not considered. It can be observed that all of the catalysts are active for the DRM. However, the CO_2 and CH_4 conversion values are lower than the thermodynamic ones in the whole temperature range, indicating the occurrence of side reactions, which were not considered for equilibrium calculations. In addition, the CO_2 conversions values are higher than those of CH_4, which indicates the presence of parallel reactions such as the RWGS and the CO disproportionation (Boudouard reaction) reactions.

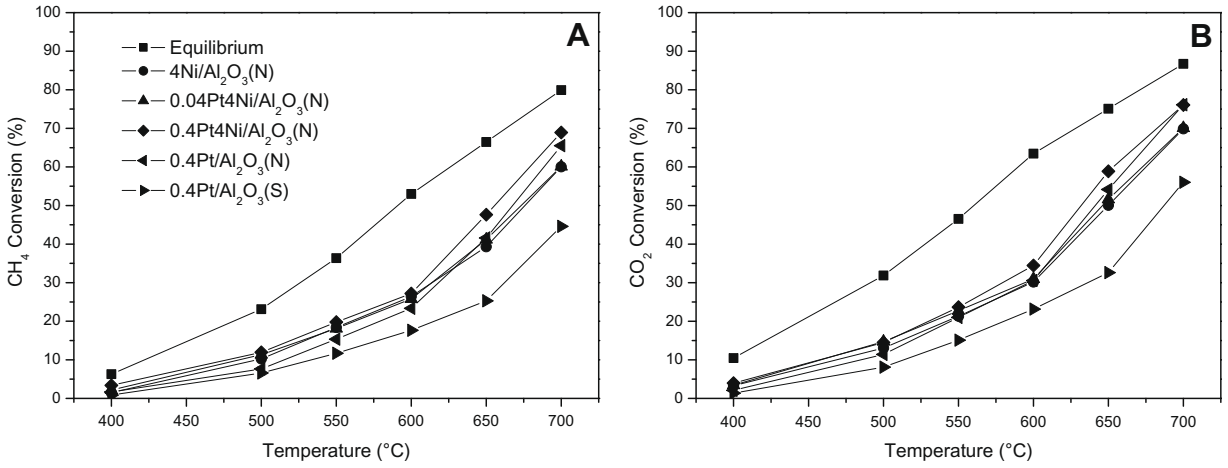

Fig. 9. CH_4 and CO_2 conversions as a function of the temperature. (A) CH_4 and (B) CO_2.

Besides, it is worth noticing that in the temperature range of 400–600 °C, there are no significant differences between the conversion values obtained with any of the PtNi catalysts. Nevertheless, in the temperature range of 600–700 °C some differences in the conversion values are appreciable, being the CO_2 and CH_4 conversions closer to the equilibrium for the catalysts that incorporate Pt. Moreover, the conversions values obtained with the 0.4Pt/Al_2O_3(S) catalyst are lower than the ones obtained with 0.4Pt/Al_2O_3(N), indicating that the nanofibrous support also affects the catalysts activity.

The selectivity values expressed as H_2/CO ratios are shown in Fig. 10. It can be observed that, as the conversion values, all of the H_2/CO ratios are lower than the equilibrium ones throughout the whole temperature range. It can also be noticeable that at low temperatures (400–600 °C) the H_2/CO ratios decrease with the Pt load. However, at 600–700 °C the H_2/CO ratios obtained with the catalysts with high Pt content show a trend toward increasing with the temperature, while the H_2/CO ratios registered with the catalysts with low Pt load tend to decrease after 600 °C.

In addition, the H_2/CO ratios at equilibrium vary almost linearly in the 500–700 °C temperature range. This is not observed in the H_2/CO curves obtained experimentally, where the curves have an inflexion point at ~600 °C; this trend is more notable for the catalysts with low Pt content (Pt/Ni = 0 and 1/100). The deviation of the H_2/CO ratios from equilibrium at high temperatures is related to the carbon formation by methane cracking and its gasification by the Boudouard reverse reaction, increasing the CO_2 and CH_4 conversions values; at high temperatures, methane cracking and carbon gasification by CO_2 are thermodynamically favored.

To determine whether the use of the nanofibrous alumina as support and the Pt content improves the Ni-Al_2O_3(N) catalysts' activity at high temperature, the H_2/CO ratios as a function of the isoconversion temperature at a CO_2 conversion (X_{CO_2}) of 60% were represented (Fig. 11). It should be pointed out that the H_2/CO ratios obtained are very close (around 0.64–0.66). However, the temperature to reach this value varies with the catalyst formulation, being lower for the catalysts supported on the Al_2O_3(N) and with high Pt content, as was expected.

Activity tests were performed at 700 °C for several hours to evaluate the catalysts' stability. The CO_2 conversion values during the first 14 h are presented in Fig. 12. It should be noted that all of the catalysts were rather stable for the DRM, with the exception of the 4Ni/Al_2O_3, for which after 14 h the CO_2 and CH_4 conversion values decreased 24% and 53%, respectively. For the Pt and Pt–Ni catalysts supported in a nanofibrous alumina, the CO_2 and CH_4 conversions values decreased 5% and 8%, respectively. The addition of Pt makes possible operation for long periods with lower carbon formation.

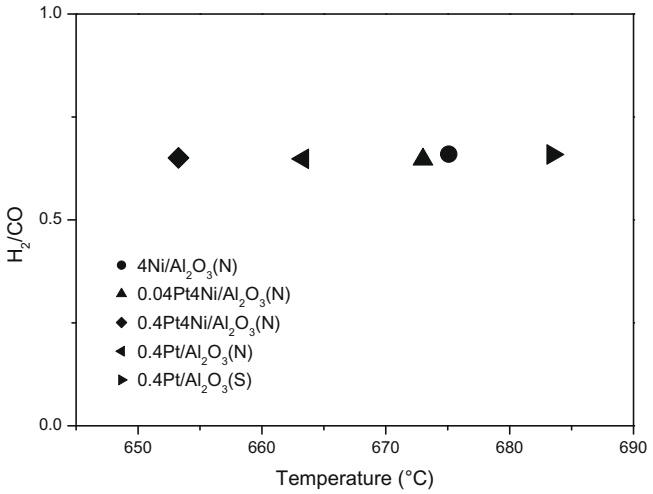

Fig. 11. H_2/CO ratio as a function of the temperature at $(X_{CO_2}) = 60\%$.

From characterization and reactivity results, it can be inferred that there is a synergic effect of the metals involved, where the PtNi catalysts tend to imitate the behavior of the Pt monometallic catalyst. For the catalyst with the lowest content of Pt (Pt/Ni = 1/100) the activity is slightly improved and the carbon formation reduced with respect to the 4Ni/Al_2O_3(N) catalysts. Moreover, for the catalysts with the highest content of Pt (Pt/Ni = 1/10) the conversions values are higher than those of the Pt/Al_2O_3(N) catalyst and the net carbon formation is almost the same.

In spite of the fact that the carbon deposition observed in the catalysts with a high Pt load was lower, its stability under dry

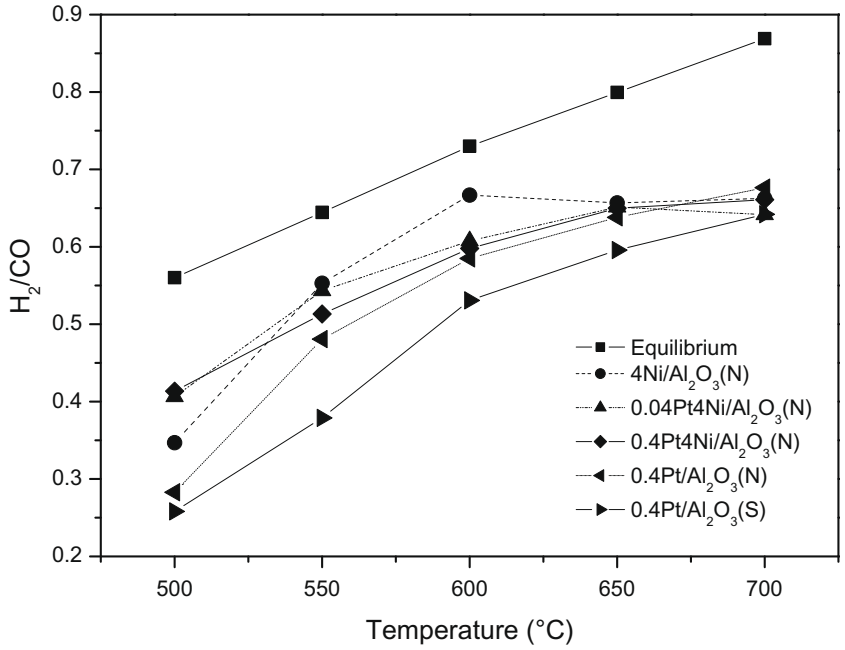

Fig. 10. H_2/CO ratio as a function of the temperature.

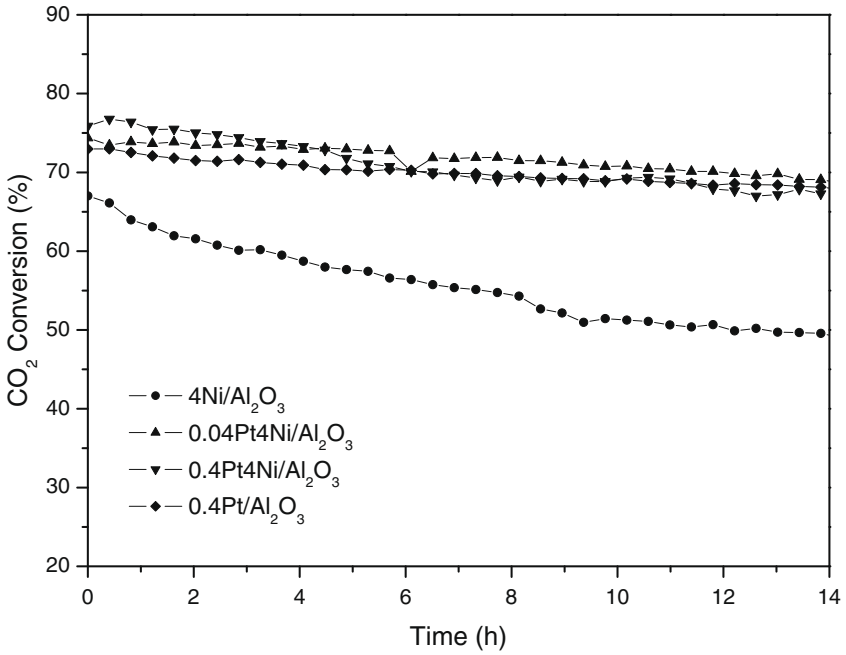

Fig. 12. CO_2 conversion vs. time on stream.

reforming of methane conditions was quite similar. This suggests that the catalysts' deactivation not only depends on the net carbon formation, but also depends on the nature of Pt–Ni and metal–support interactions, which influence the metal distribution, particle size homogeneity and nature of carbon deposition on the catalysts' surface. The carbon formation in the DRM occurs *via* two reactions: methane decomposition and CO disproportionation reactions. Methane decomposition is a structure-sensitivity reaction, which can be inhibited by controlling the catalyst surface structure. Apparently, the Pt incorporation not only conditions the Ni^0 particles size, but also avoids the Ni encapsulation by carbon. The carbon formed in the bimetallic catalysts seems to be less strongly bound to the Ni than in the $4Ni/Al_2O_3(N)$ where the carbon formed has blocked the Ni active sites. It is well known that the carbon adsorbed on small metal particles diffuses with greater difficulty than when adsorbed on large particles [22]. Additionally, carbon does not diffuse on Pt particles and almost all the carbon formed is gasified, ensuring a longer availability of active Pt sites for the DRM and keeping the activity of the Pt-containing catalysts at a constant level. The high stability and low net carbon formation in the PtNi catalysts seem to be a cooperative effect of the support and the addition of Pt, where the support allows good activity levels and high metal dispersion and reducibility, while Pt addition enhances all these effects and inhibits carbon formation.

Activity and stability results show that the nanostructured Pt–Ni catalysts might be successful catalysts with high selectivity for DRM and low selectivity toward inactive coke. Moreover, this fundamental study suggests that there is an optimum particle size and distribution of the active metal in the DRM, which will provide the best performance, the highest stability, the lowest carbon net formation and the best selectivity toward H_2 and CO.

4. Conclusions

Ni-based catalysts supported on a nanostructured alumina have proved to be highly stable and active catalysts for DRM. Even when the catalysts are prepared by the impregnation method, the morphology and the superficial characteristics of the support allow systems with homogeneous particles of Ni, which can be stabilized by Pt addition. The Pt presence in Ni-based catalysts inhibits global carbon formation, in particular the CNTs. Moreover, Pt promotes the relative content of Ni^0 and avoids Ni sintering.

The H_2/CO ratios obtained are less than one; however, the Pt–Ni nanocatalysts allow reduction in the selectivity for carbon and reach values closer to equilibrium at lower reaction temperatures. With reference to catalysts' stability, the bimetallic Pt–Ni catalysts have a good performance in the DRM at 700 °C, registering deviations less than 5% and 8% in the CO_2 and CH_4 conversions values, respectively.

Acknowledgments

M.G.D. acknowledges the Spanish Minister of Education and Science for a FPI Grant and for the financial support to the projects ENE2004-06176 and ENE2007-67926-C02-02/ALT. The authors are grateful to Prof. Ian Cooke, Dr. David Cooke and Dr. Sonia Cooke for providing language help.

References

[1] J.R. Rostrup-Nielsen, Catal. Today 18 (1993) 305.
[2] M.C.J. Bradford, M.A. Vannice, Catal. Rev. Sci. Eng. 41 (1999) 1.
[3] B. Pawelec, S. Damyanova, K. Arishtirova, J.L. Fierro, L. Petrov, Appl. Catal. A 323 (2007) 188.
[4] C.E. Daza, J. Gallego, J.A. Moreno, F. Mondragón, S. Moreno, R. Molina, Catal. Today 133–135 (2008) 357.
[5] Kee Young Koo, Hyun-Seog Roh, Yu Taek Seo, Dong Joo Seo, Wang Lai Yoon, Seung Bin Park, Appl. Catal. A 340 (2008) 183.
[6] Eli Ruckenstein, Yung Hang Hu, Appl. Catal. A 133 (1995) 149.
[7] Jeong Gil Seo, Min Hye Youn, Insung Nam, Sunhwan Hwang, Jin Suk Chung, In Kyu Song, Catal. Lett. 130 (2009) 410.
[8] N. Sahli, C. Petit, A.C. Roger, A. Kiennemann, S. Libs, M.M. Vetar, Catal. Today 113 (2006) 187.
[9] Jianguo Zhang, Hui Wang, Ajay K. Dalai, J. Catal. 249 (2007) 300.
[10] J. Wei, E. Iglesia, J. Catal. 224 (2004) 370.
[11] Yang-guang Chen, Keiichi Tomishige, Kota Yokoyama, Kaoru Fujimoto, Appl. Catal. A 165 (1997) 335.
[12] N. Wagstaff, R. Prins, J. Catal. 59 (1979) 434.
[13] C. Raab, J.A. Lercher, J.G. Goodwin, J.Z. Shyu, J. Catal. 122 (1990) 406.
[14] K. Tomishige, S. Kanazawa, M. Sato, K. Ikushima, K. Kunimori, Catal. Lett. 84 (2002) 69.
[15] Y.H. Hu, E. Ruckenstein, Adv. Catal. 48 (2004) 297.
[16] M. García-Diéguez, I.S. Pieta, M.C. Herrera, M.A. Larrubia, I. Malpartida, L.J. Alemany, Catal. Today 149 (2010) 380.

[17] N. Al-Yassir, R. Le Van Mao, Appl. Catal. A 317 (2007) 275.
[18] Agustín Martínez, Gonzalo Prieto, Joan Rollan, J. Catal. 263 (2009) 292.
[19] H.Y. Zhu, J.D. Riches, J.C. Barry, Chem. Mater. 14 (2002) 2086.
[20] M. Nowosielska, W.K. Jozwiak, J. Rynkowski, Catal. Lett. 128 (2009) 83.
[21] N.H.H. Abu Bakar, M.M. Bettahar, M. Abu Bakar, S. Monteverdi, J. Ismail, M. Alnot, J. Catal. 265 (2009) 63.
[22] J.R. Rostrup-Nielsen, Stud. Surf. Sci. Catal. 68 (1991) 85.
[23] Yueli Liu, Chunxu Pan, Jianbo Wang, J. Mater. Sci. 39 (2004) 1091.
[24] J.K.W. Sandler, S. Pegel, M. Cadek, F. Gojny, M. van Es, J. Lohmar, W.J. Blau, K. Schulte, A.H. Windle, M.S.P. Shaffer, Polymer 45 (2004) 2001.
[25] M.A. Ulla, A. Valera, T. Ubieto, N. Latorre, E. Romeo, V.G. Milt, A. Monzón, Catal. Today 133–135 (2008) 7.
[26] M. García-Diéguez, I. Pieta, F. Sánchez-García, B. Guerrero-Klein, M.C. Herrera, M.A. Larrubia, L.J. Alemany, Estudio de catalizadores soportados conteniendo Ni para el reformado seco de hidrocarburos ligeros, in: Proc. XXI Simposio Iberoamericano de Catálisis (SICAT), Málaga, 22–27 June 2008, p. 1594.
[27] Y. Schuurman, C. Marquez-Alvarez, V.C.H. Kroll, C. Mirodatos, Catal. Today 46 (1998) 185.
[28] J.Z. Shyn, K. Otto, Appl. Surf. Sci. 32 (1988) 246.
[29] J. Escard, B. Pontvianne, M.T. Chenebaux, J. Cosyns, Bull. Soc. Chim. Fr. 11 (1975) 2400.
[30] R.M. Navarro, M.C. Álvarez Galván, F. Rosa, J.L.G. Fierro, Appl. Catal. A 297 (2006) 60.
[31] C.H. Bartholomew, Catal. Rev. Sci. Eng. 24 (1982) 67.
[32] Katsutoshi Nagaoka, Kulathuiyer Seshan, Ken-ichi Aika, Johannes A. Lercher, J. Catal. 197 (2001) 34.